

## Quantum state engineering with twisted photons via adaptive shaping of the pump beam

E. V. Kovalkov,<sup>\*</sup> S. S. Straupe, and S. P. Kulik*Quantum Technologies Centre, and Faculty of Physics, M. V. Lomonosov Moscow State University, Moscow, Russia*

(Received 26 July 2018; published 12 December 2018)

High-dimensional entanglement is a valuable resource for quantum communication, and photon pairs entangled in orbital angular momentum (OAM) are commonly used for encoding high-dimensional quantum states. However, methods for the preparation of maximally entangled states of arbitrary dimensionality are still lacking, and currently used approaches essentially rely on filtering and entanglement concentration. Here, we experimentally realize a method for the generation of high-dimensional maximally entangled OAM states of photon pairs which does not require any of these procedures. Moreover, the prepared state is restricted to the subspace of the specified dimensionality, thus requiring minimal spatial postselection.

DOI: [10.1103/PhysRevA.98.060301](https://doi.org/10.1103/PhysRevA.98.060301)

The use of high-dimensional entangled systems denoted as qudits in quantum communications offers a number of advantages over the well-studied qubit systems, such as higher information capacity [1,2], enhanced robustness against eavesdropping in quantum key distribution (QKD) protocols [3], and stronger violation of generalized Bell's inequalities [4] with possible applications in device-independent QKD [5,6] and randomness generation [7]. To date, the orbital angular momentum (OAM) of light produced by spontaneous parametric down-conversion (SPDC) has become the workhorse for two-qudit state generation [8]. Twisted photons have enabled the qutrit encoding technique [9], which has been successfully used in a QKD protocol [10]. OAM of photons has recently been successfully used for three-dimensional Greenberger-Horne-Zeilinger (GHZ) state generation [11]. Although other techniques for encoding high-dimensional spatial states exist, such as, for example, multislit encoding [12], OAM-based qudits remain the only practical alternative for long-distance quantum communication in free space [13] and in multimode fibers [14].

Ideally, in a nearly collinear phase-matching geometry, the angular momentum of photons in the down-conversion process is conserved [15]. Therefore, if a pump photon has zero OAM value, the produced two-photon state is anticorrelated in OAM,

$$|\Psi\rangle = \sum_{l=-\infty}^{+\infty} c_l |l, -l\rangle. \quad (1)$$

Here,  $|c_l|^2$  determine the probabilities of finding a signal photon in the eigenstate  $|l\rangle$  carrying  $l\hbar$  units of OAM and an idler photon in the state  $|-l\rangle$  carrying  $-l\hbar$  units of OAM. The width of  $|c_l|^2$  distribution is called the spiral bandwidth and depends on the crystal length and the pump beam waist [16]. Since the amplitudes  $c_l$  are in general nonequal and decrease with increasing  $l$ , the OAM state (1) is not maximally entangled. Therefore, the generated state requires a procedure

of entanglement concentration [17] to equalize these weights [18,19]. This method (also referred to as “procrustean filtering”) implies the extraction of maximally entangled states out of nonmaximally entangled ones using spatial filtering, which inevitably leads to loss. In this Rapid Communication we present an experimental realization of maximally entangled two-qudit state generation without the need for such a filtering procedure.

It is a well-known fact that the two-photon state generated in the SPDC process carries information about the angular spectrum of the pump beam [20–23]. For example, previous experimental results have shown that the spatial mode spectrum of SPDC may be radically modified with the use of low-order Hermite-Gaussian pump beams [24,25]. Here, we go further and engineer high-dimensional states entangled in OAM with a much more complex pump beam transformation. The method we use is inspired by the theoretical work of Torres *et al.* [26], who showed that the amplitudes of the OAM-entangled quantum states can be controlled by nesting the phase singularities in the pump beam.

The analysis presented in Ref. [26] is based on the approximation of an infinite phase-matching bandwidth which implies an infinite number of spatial modes produced in SPDC. Conversely, in our approach we attempt to concentrate the full flux of the down-converted photons in the low-order mode subspace to minimize the number of unused photons. Thus, following the idea of our previous experiment [25], we first minimize the spiral bandwidth by optimal pump beam focusing. Then we reconfigure the OAM spectrum of the SPDC radiation by converting an initially Gaussian pump beam into a superposition of Laguerre-Gaussian modes  $LG_p^l$  of width  $w$ ,

$$\mathcal{E}_p(\rho, \phi; w) = \sum_l \alpha_l LG_0^l(\rho, \phi; w), \quad (2)$$

where the  $\mathcal{E}_p(\rho, \phi; w)$  function describes the electric field of the transformed beam in cylindrical coordinates  $\{\rho, \phi\}$  and  $\alpha_l$  are complex-valued coefficients. The index  $l$  is associated with an azimuthal phase term  $\exp(il\phi)$  of the LG beam and the radial index  $p$  is taken to be zero. The careful adjustment

<sup>\*</sup>ekovalkov@gmail.com

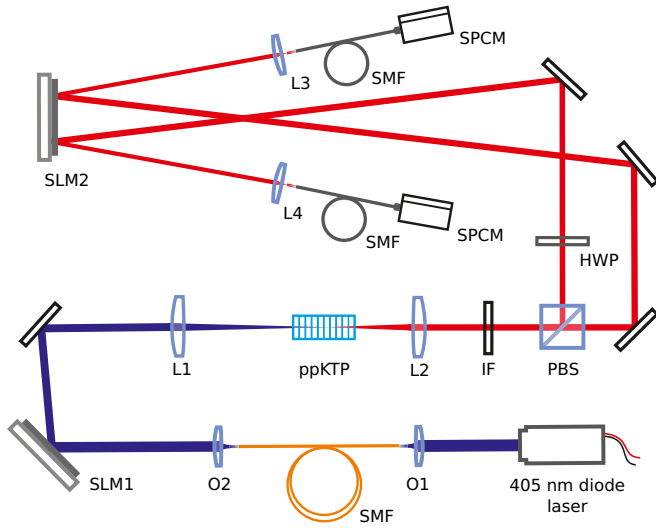


FIG. 1. Experimental setup. L1 = 200 mm, L2 = 100 mm, L3 = 44 mm, L4 = 11 mm. O1 and O2: 20 $\times$  and 10 $\times$  microscopic objectives, respectively. IF: 810  $\pm$  5-nm interference filter. SPCM: Single-photon-counting modules.

of  $\alpha_l$  allows us to control both the weights and the phases of maximally entangled high-dimensional states. Thus, the method presented here is a valuable alternative to the filtering approaches mentioned above and to the recently proposed technique of qudit generation based on entanglement by path identity [27].

*Experiment.* We use a 15-mm-thick periodically poled KTiOPO<sub>4</sub> (KTP) crystal designed for a collinear frequency degenerate type-II phase matching as a source of entangled photon pairs. The output beam of a grating-stabilized 405-nm diode laser is spatially filtered by a single-mode fiber and then shaped by the first spatial light modulator SLM1 (Cambridge Correlators). The resulting field in the first diffraction order of the SLM1 is focused on the crystal via a lens L1 (see Fig. 1 for details). Since the signal and idler photons have orthogonal polarizations, they are separated by the polarizing beam splitter (PBS). We use a well-known scheme for projective measurements in the basis of LG modes [28] by focusing the signal and idler beams on the corresponding halves of an SLM2 (Holoeye Pluto) followed by single-mode fibers and photon-counting modules. A half-wave plate (HWP) is inserted to optimize the polarization of photons reflected by the PBS for the second SLM.

Our method of hologram calculation for the LG mode generation and detection is based on the algorithm presented in Ref. [29]: The phase profile imprinted on the hologram contains the phase distribution of the desired field and a blazed grating pattern modulated by the desired amplitude distribution. This method implies that the input field is a plane wave, so its direct application to a Gaussian beam with a finite waist causes some unwanted amplitude alteration. The reverse process of mode selection with a single-mode fiber also requires us to take into account the difference between the plane wave and the fundamental fiber mode [30,31]. Thus to generate an LG mode  $\text{LG}_0^l(\rho, \phi, w) \propto (\rho/w)^{|l|} \text{L}_0^{|l|}(2\rho^2/w^2) \exp(-\rho^2/w^2) \exp(i l \phi)$  (where  $\text{L}_0^{|l|}$

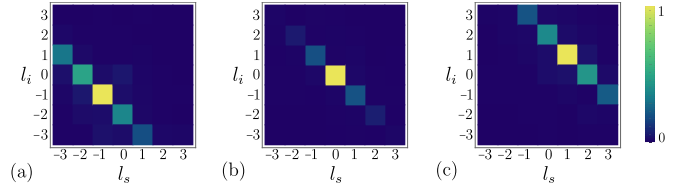


FIG. 2. Normalized (divided by the maximal value) coincidence count rates as a function of detection mode azimuthal numbers  $l_s$  and  $l_i$  for the cases of the pump beam with (a)  $l = -2$ , (b)  $l = 0$ , and (c)  $l = 2$  (experiment).

is an associated generalized Laguerre polynomial) we use a modified expression for the field imprinted on the hologram, with the modified waist  $\tilde{w}$  introduced to take into account the finite incident beam waist and to avoid amplitude alteration:  $\tilde{\text{L}}\text{G}_0^l(\rho, \phi, w, \tilde{w}) \propto (\rho/\tilde{w})^{|l|} \text{L}_0^{|l|}(2\rho^2/\tilde{w}^2) \exp(-\rho^2/w^2) \exp(i l \phi)$ . The optimal ratio  $w/\tilde{w}$  of the Gaussian and polynomial widths for the detection masks has been calculated from the experimentally determined fiber mode width and is found to be  $w/\tilde{w} = 1.6$ . The holograms displayed on the first SLM are not modified since the incident Gaussian pump beam width is significantly larger than the width of the corresponding mask.

In optimizing the regime of down-conversion for a minimal spiral bandwidth, we follow the formalism of Schmidt modes developed in Ref. [32]. According to this concept, the pump waist is chosen such that the crystal length  $L$  is approximately twice that of the Gaussian pump beam Rayleigh range. Thus we focus the pump beam to a waist size  $w = \sqrt{L/k_p} \approx 25 \mu\text{m}$ , where  $k_p$  denotes the wave vector of the pump. For the optimal detection of the down-converted modes we use the detection beam waist  $\sigma \approx 33 \mu\text{m}$ , which is close to the theoretically optimal  $\sigma = \sqrt{2}w$  for the single-Schmidt mode regime [25]. As a result, the experimentally measured azimuthal correlations between the idler and the signal channels reveal a very low contribution of the down-converted photons with  $|l| > 1$  [see Fig. 2(b)]. The number of azimuthal spatial modes can be estimated as  $K_{\text{az}} = 1/\sum_l \lambda_l^2$ , where the eigenvalues of the Schmidt decomposition  $\lambda_l$  are equal to  $|c_l|^2$  probabilities from (1) [33]. Hence, we estimate the value of  $K_{\text{az}} = 2.0 \pm 0.1$  from the diagonal distribution  $l_s = -l_i$  of measured coincidence count rates. Such a small azimuthal Schmidt number allows us to decrease the number of unused photons in high-order modes during further spiral spectrum reconfiguration.

*Qudit state engineering.* Due to the conservation of OAM, switching between an initially Gaussian pump beam and LG modes with  $l = 2$  or  $l = -2$  leads to a shift of the down-converted mode distribution from the leading diagonal  $l_s = -l_i$  to the upper diagonal  $l_s = 2 - l_i$  or subdiagonal  $l_s = -2 - l_i$ , respectively [see Figs. 2(a) and 2(c)]. Moreover, this distribution becomes wider, indicating that entanglement between spatial modes also increases with the increasing absolute value of pump OAM, being in agreement with previous experimental results [34] and our numerical calculations for the biphoton amplitude under the Gaussian approximation [32]. In particular, the predicted spiral spectra for the pump beams with  $l = -2$ ,  $l = 0$ , and  $l = 2$  approximate the

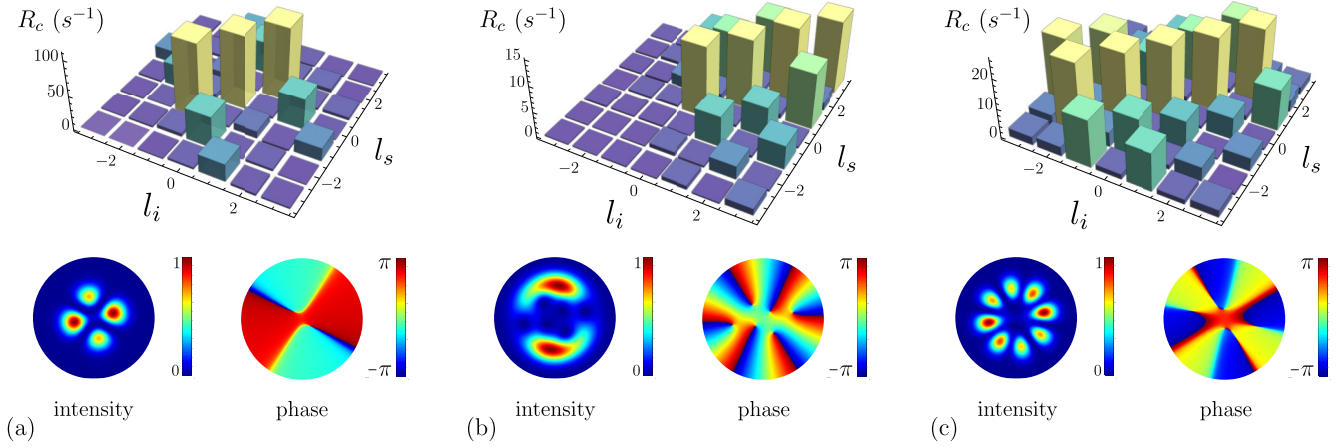


FIG. 3. Spiral spectra of maximally entangled (a) qutrits, (b) ququarts, and (c) ququints. Associated intensity and phase profiles of the pump beams calculated from the experimentally obtained coefficients  $\alpha_l$  in (2) are shown in the bottom row. The corresponding nonzero  $\alpha_l$  are (a)  $\alpha_{-2} = 0.76 - 0.11i$ ,  $\alpha_0 = -0.12 + 0.15i$ ,  $\alpha_2 = 0.30 - 0.53i$ , (b)  $\alpha_0 = 0.09 - 0.02i$ ,  $\alpha_2 = -0.02 - 0.19i$ ,  $\alpha_4 = 0.57 - 0.01i$ ,  $\alpha_6 = 0.77 - 0.21i$ , (c)  $\alpha_{-4} = -0.25 - 0.73i$ ,  $\alpha_{-2} = 0.19 - 0.10i$ ,  $\alpha_0 = -0.07 + 0.11i$ ,  $\alpha_2 = 0.14 - 0.14i$ ,  $\alpha_4 = -0.54 + 0.09i$ .

measured ones with  $R^2$  values of 0.975, 0.997, and 0.979, correspondingly. As one can see from the presented spiral spectra, the use of the pump beam in a superposition of three even low-order LG modes may provide the cross-correlation histogram with three equal antidiagonal elements, which corresponds to the generation of two maximally entangled qutrits with some phases  $\theta_1$  and  $\theta_2$ ,

$$|\Psi^{(3)}\rangle = \frac{\exp(i\theta_1)|-1, -1\rangle + |0, 0\rangle + \exp(i\theta_2)|1, 1\rangle}{\sqrt{3}}, \quad (3)$$

in the subspace  $S_3 = \{|-1, -1\rangle, |0, 0\rangle, |1, 1\rangle\}$ .

To equalize the coefficients in the generated superposition precisely and to take into account the experimental errors associated with nonperfect overlap between the pump modes and the detection modes, we further optimize the values of  $\alpha_l$  coefficients with an adaptive procedure.

For this optimization we use a simultaneous perturbation stochastic approximation (SPSA) algorithm introduced in Ref. [35]. This algorithm requires only two cost function measurements at each iteration of an optimization process, regardless of the problem dimensionality. It means that we use only two proposal vectors of modal weights  $\alpha = \{\alpha_{-2}, \alpha_0, \alpha_2\}$  and experimental estimates of the cost function to provide the direction to the optimal pump beam configuration. As a cost function  $f(\alpha)$ , we choose a variance of three measured probabilities  $|\langle l_s, l_i | \Psi^{(3)}(\alpha) \rangle|^2$  for  $l_s = l_i = -1, 0, 1$ , where the state vector of the generated state  $|\Psi^{(3)}(\alpha)\rangle = a_1(\alpha)|-1, -1\rangle + a_2(\alpha)|0, 0\rangle + a_3(\alpha)|1, 1\rangle$  depends on the vector  $\alpha$ . In other words, we seek to minimize the difference between the absolute values of the measured amplitudes  $a_i(\alpha)$  and equal weights  $1/\sqrt{3}$  to produce the maximally entangled qutrits. The resulted OAM spectrum of a maximally entangled qutrits followed by the corresponding intensity and phase profiles of the pump are shown in Fig. 3(a). A detailed description of the algorithm behavior is given in the Supplemental Material [36].

We have repeated the same procedure to produce maximally entangled ququarts by pumping the crystal with a superposition of four LG beams with even and positive

OAM values  $l = 0, 2, 4$  only. The resulting state is maximally entangled in the subspace  $S_4 = \{|0, 0\rangle, |1, 1\rangle, |2, 2\rangle, |3, 3\rangle\}$ . The corresponding beam represents a ‘‘vortex pancake’’—a Gaussian beam with phase vortices nested in it [see Fig. 3(b)]. In analogy with the previous case, we rewrite the cost function for the adaptive optimization  $f(\alpha)$  as a variance of the four measured probabilities  $|\langle l_s, l_i | \Psi^{(4)}(\alpha) \rangle|^2$  for  $l_s = l_i = 0, 1, 2, 3$  with  $\alpha = \{\alpha_0, \alpha_2, \alpha_4, \alpha_6\}$ .

Finally, we have prepared maximally entangled ququints in the subspace  $S_5 = \{|-2, -2\rangle, |-1, -1\rangle, |0, 0\rangle, |1, 1\rangle, |2, 2\rangle\}$  using a superposition of five LG beams with even  $l = -4, -2, 0, 2, 4$  as a pump. The obtained experimental results are shown in Fig. 3(c). Here, we need to note that since in the ququint case we use LG beams that have both positive and negative indices, the maximal mode order of the generated pump beam is lower than in the case of ququarts. This leads to a more efficient conversion of the initially Gaussian pump beam to the LG mode superposition despite the higher dimensionality of the prepared state. In particular, the power of the radiation incident on the crystal after the corresponding phase masks is 1.5, 0.7, and 1.1 mW for the cases of qutrits, ququarts, and ququints, respectively. At the same time, from the histograms presented in Fig. 3 we can conclude that the coincidence rates  $R_c$  for the ququint case are nearly twice as high as for the ququart one. Of course, one can use a subspace other than the proposed  $S_4$ , for example, the exclusion of any LG mode from the ‘‘ququint’’ pump seems to be a more preferable way to generate ququart states.

*Qutrit phase control.* Despite the fact that the measured spectra demonstrate the equality of the qudit amplitudes, they provide no information about the phases. Moreover, the question arises whether the pump light control allows one to produce a qudit with arbitrary phases at all. It is natural to assume that the global rotation of the pump beam does not influence the amplitudes due to the azimuthal symmetry of LG beams. According to the analytical predictions for the vortex pancake case, this statement is true [26]. At the same time, the relative phases of the components of maximally

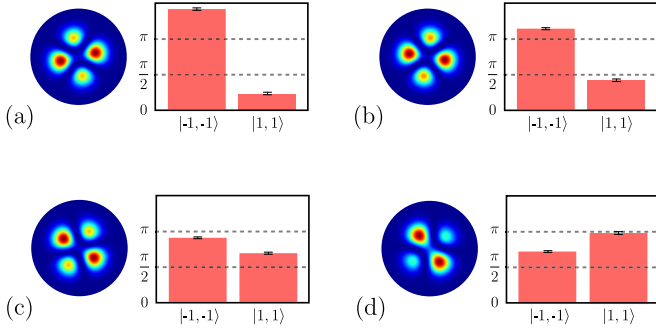


FIG. 4. Experimental phases of qutrit terms  $|-1, -1\rangle$  and  $|1, 1\rangle$  for different rotation angles (a)  $\theta = 0$ , (b)  $\theta = \pi/8$ , (c)  $\theta = \pi/4$ , and (d)  $\theta = 3\pi/8$ , followed by the corresponding intensity profiles of the pump beam. The phase of the  $|0, 0\rangle$  term is taken to be zero as a reference. Phase errors are calculated from Monte Carlo simulations of Poissonian counting statistics.

entangled states vary with the pump beam rotation angle  $\theta$  deterministically. Thus, Eq. (3) can be modified in the following way,

$$|\Psi^{(3)}(\theta)\rangle = \frac{1}{\sqrt{3}}[\exp(i\theta_1 - i2\theta)|-1, -1\rangle + |0, 0\rangle + \exp(i\theta_2 + i2\theta)|1, 1\rangle], \quad (4)$$

as a particular case of pump beam phase variation.

This prediction is in good agreement with the experiment. In order to estimate the phases of the prepared qutrits, we perform a full quantum state reconstruction in a way described in Ref. [28] for a nine-dimensional OAM subspace, spanned by all possible pairwise tensor products of  $|l\rangle$  vectors with  $l = -1, 0, 1$  (see the Supplemental Material [36] for details). Since the reconstructed density matrix  $\rho$  is mixed (as implicitly assumed by the chosen parametrization), we chose its eigenvector with the largest eigenvalue ( $\approx 0.92$ ) as an estimate of the closest pure state, and compare it with (4). The phases of  $|-1, -1\rangle$  and  $|1, 1\rangle$  terms obtained experimentally for varying  $\theta$  are presented in Fig. 4. After the rotation of the pump beam, the amplitudes of the qutrit components become slightly unequal. We launch our adaptive algorithm after each rotation by an angle  $\pi/8$  to equalize the amplitudes again. As a result, the pump beam intensity redistributes across the beam with its rotation, however, these changes are barely visible.

Arbitrary relative phases of the components may also be obtained in higher-dimensional cases by an appropriate choice of the modes' phases in the pump beam. This is confirmed by our numerical simulations. This phase control procedure is experimentally much simpler than applying mode-dependent phase shifts to the generated photon pairs, as required by existing methods.

*Entanglement verification.* To further demonstrate the entanglement of the generated qutrits, we have made use of the Collins-Gisin-Linden-Massar-Popescu (CGLMP) inequalities, which are the Bell inequalities generalized for the  $d$ -dimensional case [37]. It was shown that the Bell parameter  $I_{d=3}$  has to be less than 2 for any local realistic theory and is approximately equal to 2.87 for the case of maximally entangled qutrits. We experimentally measure the value of

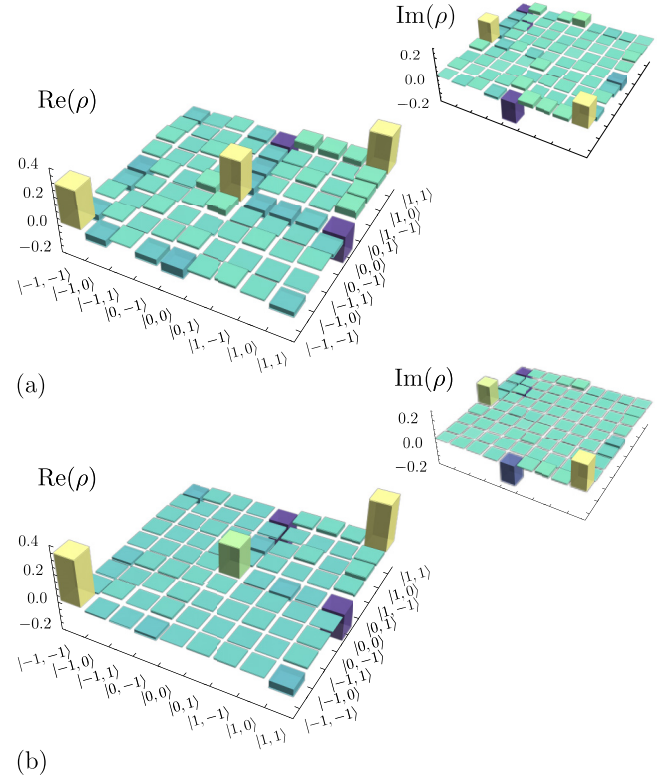


FIG. 5. Density matrices  $\rho$  of the reconstructed qutrit states. (a) A maximally entangled qutrit state, and (b) a nonmaximally entangled state from Eq. (5).

$I_3 = 2.56 \pm 0.06$ , which is well above the classical limit, but lower than the theoretical upper bound. We attribute the reduction of  $I_3$  mainly to the modest value of purity for the experimentally generated state  $\text{Tr } \rho^2 = 0.85 \pm 0.02$ . Relatively low values of purity seem to be caused by the imperfections of our mode detection technique and are ubiquitous for such realizations of projective measurements in the spatial mode basis. In addition, the grating defects in the periodically poled crystal, which are known to affect negatively the single-mode coupling efficiency [38], may also reduce the purity of the prepared state.

It is well known that the CGLMP inequalities for the dimensionality  $d > 2$  are maximally violated by nonmaximally entangled states. In particular, for qutrits the maximal violation is obtained for states of the form

$$|\Psi\rangle = 1/\sqrt{2 + \gamma^2}(|-1, -1\rangle + \gamma|0, 0\rangle + |1, 1\rangle). \quad (5)$$

The maximal value of  $I_3 \approx 2.91$  corresponds to  $\gamma \approx 0.79$  [39]. To demonstrate the capability of our technique we prepared this state experimentally, however, we were not able to significantly improve the violation—the experimental value of  $I_3 = 2.61 \pm 0.05$  is equal to that of maximally entangled states within experimental uncertainty. This value is in agreement with theoretical predictions for the uncolored noise model  $\rho = p|\psi\rangle\langle\psi| + (1-p)\mathbb{1}/d^2$ , where the  $I_3$  parameter scales as  $pI_3$ . The experimentally obtained  $p = 0.91 \pm 0.02$  and  $p = 0.88 \pm 0.02$  for the maximally and nonmaximally

entangled states, correspondingly, explain well the observed reduction of  $I_3$ , which was also reported before in other experiments [40]. The results of the experimental state reconstructions of maximally entangled and nonmaximally entangled qutrit states are shown in Fig. 5.

*Discussion.* We have experimentally demonstrated a method for the generation of spatially entangled states of photons with variable dimensionality. In this Rapid Communication we mostly focused on generating maximally entangled states with equal amplitudes of the components in the superposition, however, the method is completely general, and may be used to generate qudit states with an arbitrary distribution of amplitudes and phases. The level of control over generated states demonstrated here is sufficient, for example, to generate all mutually unbiased bases for a realization of a high-dimensional QKD protocol [1,3]. Moreover, the adaptive procedure used here to supplement the analytical heuristic may be utilized on its own to generate completely arbitrary spatial states of photon pairs, with the only limitation being the conservation laws in the SPDC process. For example,

one may use full-state tomography to estimate the fidelity of the prepared state with the desired one, and use it as a cost function for the optimization routine. We believe that this approach may become an interesting and fruitful research direction.

Despite the fact that our method does not require the procedure of entanglement concentration, the prepared states still have to be postselected to belong to the subspace of OAM modes spanned by  $|l, l\rangle$  products, since the two-dimensional spiral spectra in Fig. 3 contain a significant amount of unwanted components for the unequal  $l_s$  and  $l_i$ . However, these distributions might be diagonalized by the transition from the OAM measurement basis to the eigenbasis of the produced state density matrix, i.e., the true Schmidt modes [41]. This possibility will be explored elsewhere.

*Note added.* Recently, we became aware of a closely related work [42].

*Acknowledgments.* This work was supported by the Russian Science Foundation Project No. 16-12-00017. E.V.K. acknowledges support from the BASIS Foundation.

- 
- [1] H. Bechmann-Pasquinucci and W. Tittel, *Phys. Rev. A* **61**, 062308 (2000).
  - [2] S. P. Walborn, D. S. Lemelle, M. P. Almeida, and P. H. Souto Ribeiro, *Phys. Rev. Lett.* **96**, 090501 (2006).
  - [3] N. J. Cerf, M. Bourennane, A. Karlsson, and N. Gisin, *Phys. Rev. Lett.* **88**, 127902 (2002).
  - [4] D. Kaszlikowski, P. Gnaniński, M. Żukowski, W. Miklaszewski, and A. Zeilinger, *Phys. Rev. Lett.* **85**, 4418 (2000).
  - [5] J. Barrett, L. Hardy, and A. Kent, *Phys. Rev. Lett.* **95**, 010503 (2005).
  - [6] U. Vazirani and T. Vidick, *Phys. Rev. Lett.* **113**, 140501 (2014).
  - [7] A. Acín and L. Masanes, *Nature (London)* **540**, 213 (2016).
  - [8] M. Erhard, R. Fickler, M. Krenn, and A. Zeilinger, *Light: Sci. Appl.* **7**, 17146 (2018).
  - [9] A. Vaziri, G. Weihs, and A. Zeilinger, *Phys. Rev. Lett.* **89**, 240401 (2002).
  - [10] S. Gröblacher, T. Jennewein, A. Vaziri, G. Weihs, and A. Zeilinger, *New J. Phys.* **8**, 75 (2006).
  - [11] M. Erhard, M. Malik, M. Krenn, and A. Zeilinger, *arXiv:1708.03881*.
  - [12] L. Neves, G. Lima, J. G. Aguirre Gómez, C. H. Monken, C. Saavedra, and S. Pádua, *Phys. Rev. Lett.* **94**, 100501 (2005).
  - [13] M. Krenn, J. Handsteiner, M. Fink, R. Fickler, and A. Zeilinger, *Proc. Natl. Acad. Sci. USA* **112**, 14197 (2015).
  - [14] A. E. Willner, H. Huang, Y. Yan, Y. Ren, N. Ahmed, G. Xie, C. Bao, L. Li, Y. Cao, Z. Zhao *et al.*, *Adv. Opt. Photonics* **7**, 66 (2015).
  - [15] A. Mair, A. Vaziri, G. Weihs, and A. Zeilinger, *Nature (London)* **412**, 313 (2001).
  - [16] J. P. Torres, A. Alexandrescu, and L. Torner, *Phys. Rev. A* **68**, 050301 (2003).
  - [17] C. H. Bennett, H. J. Bernstein, S. Popescu, and B. Schumacher, *Phys. Rev. A* **53**, 2046 (1996).
  - [18] A. Vaziri, J.-W. Pan, T. Jennewein, G. Weihs, and A. Zeilinger, *Phys. Rev. Lett.* **91**, 227902 (2003).
  - [19] A. C. Dada, J. Leach, G. S. Buller, M. J. Padgett, and E. Andersson, *Nat. Phys.* **7**, 677 (2011).
  - [20] A. V. Burlakov, M. V. Chekhova, D. N. Klyshko, S. P. Kulik, A. N. Penin, Y. H. Shih, and D. V. Strekalov, *Phys. Rev. A* **56**, 3214 (1997).
  - [21] C. H. Monken, P. H. Souto Ribeiro, and S. Pádua, *Phys. Rev. A* **57**, 3123 (1998).
  - [22] S. P. Walborn, A. N. de Oliveira, R. S. Thebaldi, and C. H. Monken, *Phys. Rev. A* **69**, 023811 (2004).
  - [23] D. Ghosh, T. Jennewein, P. Kolenderski, and U. Sinha, *OSA Continuum* **1**, 996 (2018).
  - [24] J. Romero, D. Giovannini, M. McLaren, E. Galvez, A. Forbes, and M. Padgett, *J. Opt.* **14**, 085401 (2012).
  - [25] E. V. Kovlakov, I. B. Bobrov, S. S. Straupe, and S. P. Kulik, *Phys. Rev. Lett.* **118**, 030503 (2017).
  - [26] J. P. Torres, Y. Deyanova, L. Torner, and G. Molina-Terriza, *Phys. Rev. A* **67**, 052313 (2003).
  - [27] M. Krenn, A. Hochrainer, M. Lahiri, and A. Zeilinger, *Phys. Rev. Lett.* **118**, 080401 (2017).
  - [28] M. Agnew, J. Leach, M. McLaren, F. S. Roux, and R. W. Boyd, *Phys. Rev. A* **84**, 062101 (2011).
  - [29] E. Bolduc, N. Bent, E. Santamato, E. Karimi, and R. W. Boyd, *Opt. Lett.* **38**, 3546 (2013).
  - [30] Y. Zhang, F. S. Roux, M. McLaren, and A. Forbes, *Phys. Rev. A* **89**, 043820 (2014).
  - [31] F. Bouchard, N. H. Valencia, F. Brandt, R. Fickler, M. Huber, and M. Malik, *Opt. Express* **26**, 31925 (2018).
  - [32] C. K. Law and J. H. Eberly, *Phys. Rev. Lett.* **92**, 127903 (2004).
  - [33] F. M. Miatto, H. D. L. Pires, S. M. Barnett, and M. P. van Exter, *Eur. Phys. J. D* **66**, 263 (2012).
  - [34] F. Bouchard, J. Harris, H. Mand, N. Bent, E. Santamato, R. W. Boyd, and E. Karimi, *Sci. Rep.* **5**, 15330 (2015).
  - [35] J. C. Spall, *IEEE Trans. Aerosp. Electron. Syst.* **34**, 817 (1998).
  - [36] See Supplemental Material at <http://link.aps.org/supplemental/10.1103/PhysRevA.98.060301> for a detailed discussion of

- optimization algorithm, Bell inequalities for qutrits, maximally entangled qubit phase control, and full-state tomography of the entangled qutrit state, which includes Refs. [25,35,37,43].
- [37] D. Collins, N. Gisin, N. Linden, S. Massar, and S. Popescu, *Phys. Rev. Lett.* **88**, 040404 (2002).
- [38] A. Fedrizzi, T. Herbst, A. Poppe, T. Jennewein, and A. Zeilinger, *Opt. Express* **15**, 15377 (2007).
- [39] A. Acin, T. Durt, N. Gisin, and J. I. Latorre, *Phys. Rev. A* **65**, 052325 (2002).
- [40] C. Bernhard, B. Bessire, T. Feurer, and A. Stefanov, *Phys. Rev. A* **88**, 032322 (2013).
- [41] G. Patera, C. Navarrete-Benlloch, G. J. de Valcárcel, and C. Fabre, *Eur. Phys. J. D* **66**, 241 (2012).
- [42] S.-L. Liu, Z.-Y. Zhou, S.-K. Liu, Y.-H. Li, Y. Li, C. Yang, Z.-h. Xu, Z.-d. Liu, G.-C. Guo, and B.-S. Shi, *Phys. Rev. A* **98**, 062316 (2018).
- [43] D. F. V. James, P. G. Kwiat, W. J. Munro, and A. G. White, *Phys. Rev. A* **64**, 052312 (2001).